MULTIPLE-IMAGE COMPUTED TOMOGRAPHY*

Jovan G. Brankov[1], Miles N. Wernick[1,4], Dean Chapman[2], Zhong Zhong[3], Carol Muehleman[5], Jun Li[5], Mark A. Anastasio[4]

[1] Department of Electrical and Computer Engineering, Illinois Institute of Technology, Chicago, IL 60616, USA
[2] Department of Physics, Illinois Institute of Technology, Chicago, IL 60616, USA
[3] National Synchrotron Light Source, Brookhaven National Laboratory, Upton, NY 11973, USA
[4] Department of Biomedical Engineering, Illinois Institute of Technology, Chicago, IL 60616, USA
[5] Rush Medical College, Chicago, IL

ABSTRACT

We have recently proposed and investigated a planar imaging method called multiple-image radiography (MIR) that concurrently produces three two-dimensional images that reveal information about the ultra-small-angle scattering and refractive index properties of the object, in addition to an almost scatter-free radiographic image that depicts the projected absorption properties of the object. In this work, we develop and implement experimentally a computed tomography (CT) version of MIR, referred to as multiple-image CT (MICT), that produces three volumetric images of these object properties. The appropriateness of a linear imaging model is validated experimentally by use of phantom studies. The MICT method is employed for reconstruction of images of two biological phantoms using measurement data produced by a synchrotron light source.

1. INTRODUCTION

The development and investigation of X-ray imaging techniques that exploit contrast mechanisms other than x-ray absorption has become an active and important research area. Because of their ability to distinguish between structures that have very similar or identical absorption properties (e.g. soft-tissue structures), these imaging techniques hold great promise for benefiting many clinical and biological imaging applications.

We have recently proposed and investigated a new planar imaging method called *multiple-image radiography* (MIR) [1] that produces a comprehensive description of an object's absorption, refraction and ultra-small-angle scattering properties. The MIR imaging technique is a generalization of the diffraction-enhanced imaging (DEI) method that has been investigated extensively in recent years [2], and is qualitatively similar to an analyzer-based x-ray imaging technique proposed recently by Pagot *et al*. [3]. The hardware devices and experimental conditions that are needed to implement MIR are essentially the same as those needed in DEI; these include a monochromatic X-ray beam that is used to irradiate the object and an analyzer crystal, placed between the object and a detector system, that can reveal information regarding certain diffracted (or multiply-refracted) components of the transmitted beam. As in DEI, MIR produces an image representing a projected refractive index gradient distribution and a second image that is an X-ray radiograph. However, the radiograph produced in MIR (and DEI) will contain a negligible contribution from non-primary photons due to the scatter rejection properties of the analyzer crystal. Unlike in DEI, the MIR method produces a third image that represents the ultra-small-angle scattering properties of the object. This image reveals textural features of the object, and provides important information about the object's physical properties that is complementary to that conveyed by the refraction- and absorption-based images.

Although the three parametric images produced in MIR provide a rich description of the object's physical properties, they are two-dimensional (2D) images that represent projections of the three-dimensional (3D) object properties. The motivations for extending MIR into a 3D computed tomography (CT) imaging method are compelling. In addition to the 3D X-ray attenuation coefficient distribution, MIR operating in CT-mode, which we will refer to as multiple-image CT (MICT), can produce 3D spatial maps of the refraction and ultra-small-angle scattering properties of the object. These images convey potentially useful information about object properties that are not measured in conventional x-ray CT. Moreover, the spatial correlation of information contained in the three volumetric images can provide a informative characterization of the object that may significantly improve the accuracy of diagnostic tasks.

In this work we develop and implement the MICT imaging method. Motivated by the linearity of the MIR imaging model, we utilize the 2D filtered backprojection (FBP) algorithm for reconstructing transverse slices of 3D images that accurately represent the absorption, refractive index gradient, and ultra-small-angle scattering properties of an object. The

* This research was supported by NIH/NIAMS grant AR48292.

appropriateness of the linear imaging model (i.e., X-ray transform) is validated experimentally by use of phantom studies. The MICT method is employed for reconstruction of two biological phantoms using measurement data produced by a synchrotron light source.

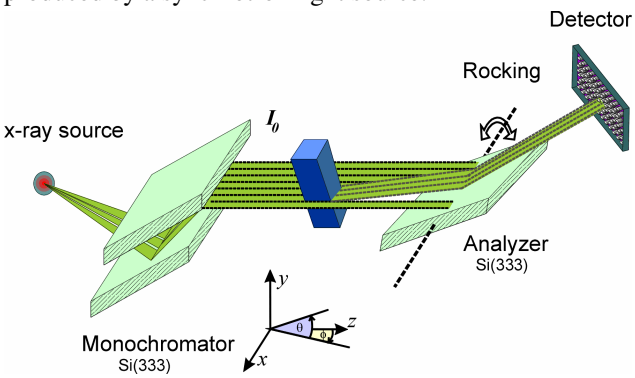

Fig1. Illustration of the imaging system used by MIR and MICT. In order to analyze the angular intensity spectrum of the transmitted beam the analyzer crystal is rotated (rocked).

2. PLANAR MIR IMAGING MODEL

The three planar images produced in MIR are obtained by use of a system of diffractive optical elements that allows the angular content of the beam to be analyzed. As shown in Figure 1, the object is irradiated by a collimated, monochromated X-ray beam that travels along the positive z-axis. After passing through the object, the transmitted beam is incident on an analyzer crystal that reflects only those components of the beam traveling at an angle θ that equals, or is very close to, the analyzer's Bragg angle. Therefore, the analyzer crystal allows one to isolate approximately the components of the transmitted beam that are propagating in a specified direction. Note that in MIR, the transmitted beam components travel at angles described by extremely small values of θ (on the order of microradians) with respect to the optical axis of the imaging system. By rotating the analyzer crystal with respect to the angle θ and acquiring multiple images along the way, it is possible to gain the information needed to compute the intensity and directionality characteristics of the transmitted beam. As described in Section 3, such information permits for the computation of parametric images that represent the absorption, refractive, and ultra-small-angle scattering properties of the object.

Using the same assumptions as transport theory [4], we will treat beam propagation through the object as linear in intensity. Therefore, the effect of the object on the beam can be regarded as a linear system in terms of the angle θ. Furthermore, we assume that the angular intensity spectrum of each sub-pixel region in the object is nearly independent of θ. In this case, one obtains the imaging model [1]:

$$f(\theta;x,y) = R(\theta) * g(\theta;x,y), \quad (1)$$

where $*$ represent a 1D convolution over θ, $f(\theta;x,y)$ is the measured angular intensity spectrum at pixel location (x,y), $g(\theta;x,y)$ represent the impulse response of the object, and $R(\theta)$ is the intrinsic rocking curve of the imaging system. Note that $R(\theta)$ represents the angular intensity spectrum that would be measured in the absence of the object and $g(\theta;x,y)$ represents the angular intensity spectrum of the transmitted beam that would be produced if the object were illuminated by plane-wave.

The discrete form of Eq. (1) is given by

$$f_{m,n}[k] = R[k] * g_{m,n}[k], \quad (2)$$

where the detector pixels are referenced by the spatial indices $m = 1,2,...,M$ and $n = 1,2,...,N$, and $k = 1,2,...,K$ describe discrete (angular) analyzer crystal settings. Therefore, at each pixel location (m,n) on the detector, we measure the angular intensity spectrum $f_{m,n}[k]$ at the K angular settings of the analyzer crystal. The measured data set is consequently composed of K images, each of dimension $M \times N$.

The information contained in the measured angular intensity spectrum $f_{m,n}[k]$ can be conveniently summarized by computing parametric images that reflect the attenuation, refraction, and ultra-small-angle scattering properties of the object. The computation of the parametric images from knowledge of $f_{m,n}[k]$ are described below. Before doing so, it will be useful to define the following intermediate quantities. Let the total intensity at a given pixel (m,n) be denoted by

$$T_{m,n} = \sum_{k=1}^{K} f_{m,n}[k], \quad (3)$$

and define a normalized angular intensity spectrum as

$$F_{m,n}[k] = \frac{f_{m,n}[k]}{T_{m,n}}. \quad (4)$$

Without loss of generality we will assume that imaging system angular spectrum has a zero shift. i.e.:

$$\sum_{k=1}^{K} \theta_k R[k] = 0. \quad (5)$$

where θ_k are the angular sample points at which data are recorded.

2.1. Attenuation image.

The first parametric image represents attenuation of the x-ray beam that is caused by absorption and scattering into

angles outside the measured angular range. These sources of beam attenuation are collectively summarized by the image:

$$\hat{a}_{m,n} = -\ln T_{m,n}\,, \tag{6}$$

which is simply a discrete inversion of an exponential loss law.

2.2. Refraction image.

The second parametric image represents the refractive properties of the object. Refraction due to variations in the x-ray refractive index distribution induces an overall deflection of the beam. This deflection is measured as the angular shift of the beam centroid, as compared to its position when no object is present, which is computed as

$$r_{m,n} = \sum_{k=1}^{K} \theta_k F_{m,n}[k]\,. \tag{7}$$

2.3. Ultra-small-angle scatter image.

The third parametric image represents the ultra-small-angle scattering properties of the object. Ultra-small-angle scatter by sub-pixel-sized object structures causes an angular broadening of the transmitted beam. This angular broadening can be described by the beam's angular divergence about the angle $r_{m,n}$, as measured by the second central moment of the normalized angular intensity spectrum as

$$s_{m,n} = \sum_{k=1}^{K} \left(\theta_k - r_{m,n}\right)^2 \left(F_{m,n}[k] - R[k]\right) \tag{8}$$

If an explicit deconvolution step were performed as in [1] this term would vanish.

2.4. Alternative approach to analyze angular intensity spectrum

In some situations, the direct calculation of the above parametric images could lead to significant inaccuracies. These inaccuracies could result, for example, from an insufficient sampling density in the angular coordinate of the measured data functions. To circumvent such problems, our group has proposed an alternative approach for estimation of beam parameters that is based on a curve-fitting method [5].

3. MICT IMAGING

As defined earlier, we will refer to MIR imaging operating in CT mode as MICT. In MICT, the object is placed on a rotation stage whose rotation axis is parallel to the y-axis. (Conversely, one can imagine that the object is held fixed and the x-ray source, crystal optics, and detector are simultaneously rotated about the y-axis.) At each tomographic view angle, the MIR method is implemented and the three parametric images are computed as described by Eqs. (6-8). As discussed below, each parametric image can be interpreted as the projection (i.e., a 3D x-ray transform with a circular source trajectory or a stack of 2D Radon transforms along the y-axis) of its associated object property distribution. As such, by considering the sets of measurements acquired at all view angles, we can reconstruct volumetric images that represent the attenuation, refractive, and ultra-small-angle-scattering object properties by use of the 2D filtered backprojection (FBP) algorithm.

The linear tomographic model described above is a direct consequence of the convolutional form of the MIR imaging model given in Eq. (1). The fact that the attenuation and refractive index gradient images are linearly related to the attenuation and refraction parametric images is not surprising; The attenuation parametric image is defined as an inversion of an exponential loss law and can therefore be related immediately to line integrals of an attenuation distribution. Under a geometrical optics description of the beam propagation though the object, which is very appropriate in MIR imaging, the refraction image can be shown to be related to a derivative (with respect to y) of line integrals through the x-ray refractive index distribution of the object [6]. In situations where scattering in the material can be described by Gaussian phase functions, it can be also be shown that the ultra-small-angle scatter image is linearly related to the scattering properties of the object [4].

Because it is the object property that we have the least experience with, an experiment was designed to demonstrate linearity of the ultra-small-scatter parameter $s_{m,n}$. A lucite wedge was filled with a mixture of glycerin and micro-spheres. The mean diameter of microspheres was 6.5 μm. The volumetric density of microspheres was 10^9cm^{-3} and imaging was performed at an x-ray energy of 18 keV. The results of this experiment show that the ultra-small-scatter parameter is linear as a function of the sample thickness. The data were found to fit a linear model (using a least-squares criteria) with a significance level of $p \le 10^{-4}$.

4. EXPERIMENT: MICT IMAGING

4.1. Phantom experiment

A phantom, shown in Figure 2(a), consisting of a Lucite jar containing a tilted Lucite rod and a sheet of paper rolled into a cylinder was used to demonstrate experimentally the MICT method. The imaging was performed using 40 keV x-rays at the National Synchrotron Light Source X15A imaging beamline. The object was rotated in one degree increments over a 360 degree range. At each view angle, the angular intensity spectrum was measured at 11 analyzer positions, ranging from -4 to $+4\mu$rad with 0.8μrad increments. Each

image consisted of 1256×444 pixels with size $50\mu\text{m}\times50\mu\text{m}$.

The reconstructed MICT images representing attenuation, refraction, and ultra-small-angle scatter are presented in Figure 2 (left, center, and right), respectively. In this simple phantom, paper is easily distinguished, as expected, by its high values in the scatter image. The surface of the rod is identified by high values at its surface in the refraction image. The Lucite jar only appears significantly in the attenuation image.

4.2. Talus bone experiment

To demonstrate the potential of MICT for medical imaging, the head of a single human talus bone of the ankle joint was imaged. The MICT results are presented in Figure 3. Our preliminary investigation of these images suggests that, while the attenuation image reflects the same information as conventional x-ray radiography, the refraction and scatter images reveal additional potentially useful information. Although the articular cartilage covering the articular surface of the head of the talus is faintly visible in the attenuation image, it is clearly visible in the refraction and scatter images (between arrows). This is of clinical significance because cartilage is invisible on conventional radiographs. The clinical utility of MICT remains an important topic for future investigation.

5. CONCLUSION

We have developed and implemented experimentally a novel CT imaging method that we call multiple-image CT (MICT). MICT is a tomographic extension of MIR, and is capable of reconstructing volumetric images that represent the absorption, refractive, and ultra-small-angle scattering properties of an object. In future studies, we plan to formalize the MIR and MICT imaging models by use of scattering theory. We also will investigate clinical applications of MICT.

6. REFERENCES

[1] M. N. Wernick *et al,* "Multiple-image radiography," *Phys. Med. Biol.,* vol. 48, pp. 3875-3895, 2003.

[2] D. Chapman *et al*, "Diffraction Enhanced X-ray Imaging," *Phys. Med. Biol*., vol. 42, pp. 2015-2025, 1997.

[3] E. Pagot *et al*, "A method to extract quantitative information in analyzer-based x-ray phase contrast imaging," *App. Phys. Letters*, vol. 82, pp. 3421-3423, 2003.

[4] A. Ishimaru, *Wave Propagation and Scattering in Random Media,* Piscataway, New Jersey, 1997.

[5] O. Oltulu *et al,* "Extraction of extinction, refraction and absorption properties in diffraction enhanced imaging," *J. Phys. D: Appl. Phys.,* vol. 36, pp. 2152–62, 2003.

[6] F. A. Dilmanian *et al* "Computed tomography of x-ray index of refraction using the diffraction enhanced imaging method," *Phys. Med. Biol.* vol. 45, pp.933–46, 2000.

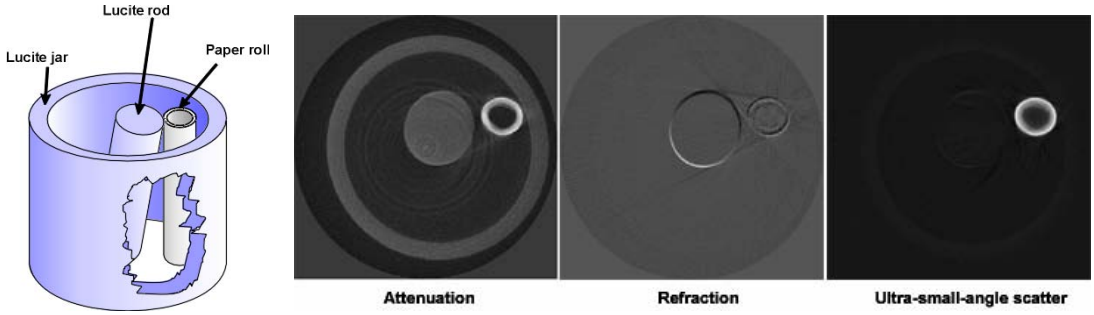

Figure 2. Phantom used in MICT study and MICT images. As expected, the Lucite rod produces substantial refraction, but little scatter; the converse is true of the paper roll.

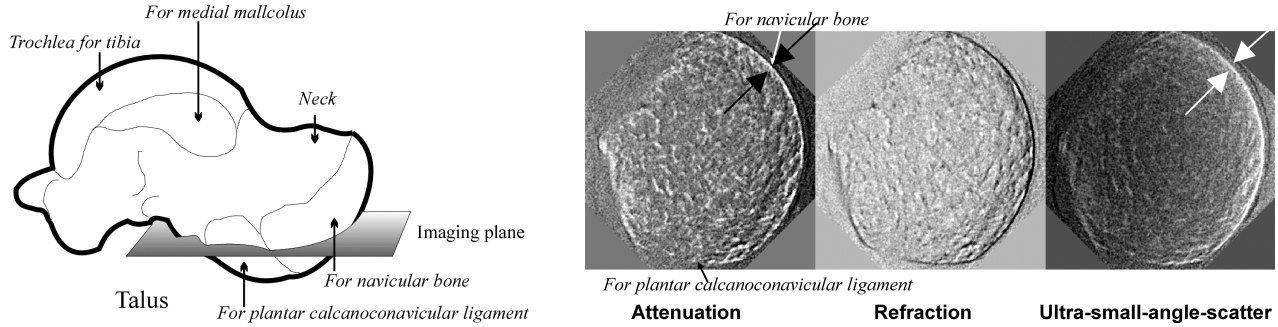

Figure 3. MICT images of a human bone.